On the Physical Meaning of Single-Value Activation Energies for BTI in Si and SiC MOSFET Devices

M. W. Feil, K. Puschkarsky, *Member, IEEE*, W. Gustin, H. Reisinger, and T. Grasser, *Fellow, IEEE*

***Abstract*—Bias temperature instability (BTI) has been shown to be the collective response of an ensemble of defects to a gate voltage signal. Each defect can be described using first-order reactions for either charge trapping or defect creation with a broad distribution of time constants. Consequently, the temperature dependence of BTI has to be determined by a distribution of activation energies reflecting the variety of available defects. Commonly employed single-value apparent activation energy-based modeling of BTI can therefore be at best a very rough approximation and its apparent activation energy is consequently a model parameter without physical justification. This study investigates the impact of measurement parameters, such as the extraction point in the drift curve and the recovery time, on these apparent activation energies that can be extracted either by threshold voltage shift increase (vertical method) or by stress time acceleration (horizontal method). The framework of activation energy maps enables an analytical mathematical approach to calculate the dependence of extracted apparent activation energies on the measurement parameters. A comparison between Si and SiC MOSFET devices is employed, and nonphysical negative apparent activation energies are explained. Since apparent activation energies have been repeatedly employed to justify physics-based descriptions of BTI, their physical (in)significance is discussed.**

***Index Terms*—Activation energy maps (AE maps), apparent activation energy, Arrhenius law, bias temperature instability (BTI), modeling, recovery.**

I. Introduction

ACTIVATION energies are commonly employed to account for the temperature dependence of bias temperature instability (BTI) that is a degradation mechanism in MOSFETs leading to device parameter shifts upon gate voltage stress [1]–[3]. The relationship between threshold voltage shift and stress time is often empirically modeled with a power law

$$\Delta V_{\rm th} = C t_{\rm s}^{n} \tag{1}$$

with C as a temperature- and bias-dependent prefactor and $t_{\rm s}$ as the stress time. The time exponent n is usually assumed to be temperature and stress time independent and is typically in the range of 0.1–0.3 [2]. Note that the assumption of time-independent n does not hold for all time scales, as the degradation has been shown to saturate [4], [5]. In most cases, the stress time dependence of the threshold voltage shift is determined by measure-stress-measure (MSM) schemes with single or extended threshold voltage readouts [6] consisting of increasing stress periods that are interrupted for recovery phases during which the threshold voltage is measured and compared to an initial reference. A detailed discussion of different measurement techniques typically used for Si and SiC MOSFETs can be found in [7]. Accordingly, temperature dependence of BTI is monitored by performing the MSM schemes at different temperatures, e.g., at T_1 and T_2, and modeled by introducing an apparent activation energy. This apparent activation energy is commonly extracted in two different ways. The conventional vertical extraction method determines an apparent activation energy $E_{\rm a,V}^{\rm app}$ by the temperature-induced change of the threshold voltage shift $\Delta V_{\rm th}$ after a certain stress time [see Fig. 1(a)]

$$E_{\rm a,V}^{\rm app} = k_{\rm B}\frac{T_1\ T_2}{T_2 - T_1}\ln\left(\frac{\Delta V_{\rm th}(T_2)}{\Delta V_{\rm th}(T_1)}\right). \tag{2}$$

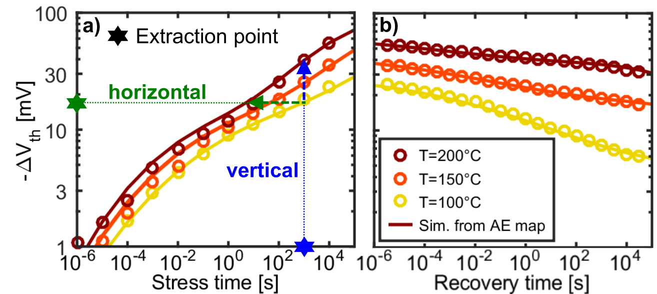

Fig. 1. Measured threshold voltage shift $\Delta V_{\rm th}$ from a silicon technology with a stress voltage of $V_{\rm GS} = -2$ V at three different temperatures. Solid lines indicate the drift values resulting from a simulation based on the AE map in Fig. 2 [8]. (a) Stress time dependence at a constant recovery time of $t_{\rm r} = 1$ µs. (b) Recovery time dependence after a stress time of $t_{\rm s} = 10^4$ s.

Manuscript received September 8, 2020; revised October 20, 2020; accepted October 29, 2020. Date of publication November 26, 2020; date of current version December 24, 2020. The review of this article was arranged by Editor N. Xu. *(Corresponding author: M. W. Feil.)*

M. W. Feil and K. Puschkarsky are with the Institute for Microelectronics, TU Wien and Infineon Technologies AG, 85579 Neubiberg, Germany (e-mail: maximilian.feil@infineon.com).

W. Gustin and H. Reisinger are with Infineon Technologies AG, 85579 Neubiberg, Germany.

T. Grasser is with the Institute for Microelectronics, TU Wien, 1040 Vienna, Austria (e-mail: grasser@iue.tuwien.ac.at).

Color versions of one or more figures in this article are available at https://doi.org/10.1109/TED.2020.3036321.

Digital Object Identifier 10.1109/TED.2020.3036321

0018-9383 © 2020 IEEE. Personal use is permitted, but republication/redistribution requires IEEE permission.
See https://www.ieee.org/publications/rights/index.html for more information.

Authorized licensed use limited to: TU Wien Bibliothek. Downloaded on January 05,2021 at 07:18:06 UTC from IEEE Xplore. Restrictions apply.

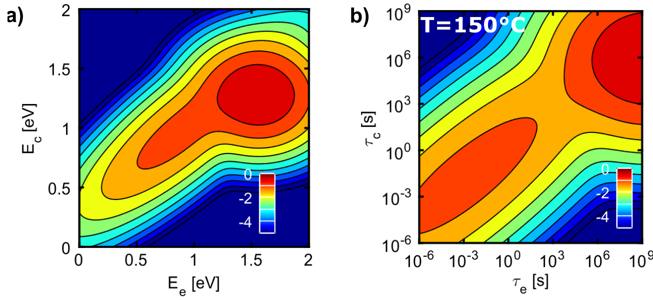

Fig. 2. AE and CET maps of a silicon technology extracted from the data presented in [8] for $V_{GS} = -2$ V. Both maps are shown on a logarithmic color scale. A density value of x corresponds to ΔV_{th} of 10^x V eV^{-2} and 7×10^x mV. (a) AE map for the recoverable and quasi-permanent component. (b) CET map at $T = 150$ °C calculated from (a). Note that the shown density values are per squared decade in time.

In contrast, the horizontal extraction method determines an apparent activation energy $E_{a,H}^{app}$ from the temperature induced change in time t_s needed to reach the same threshold voltage shift [see Fig. 1(a)]

$$E_{a,H}^{app} = k_B \frac{T_1\ T_2}{T_2 - T_1} \ln\left(\frac{t_{s,1}}{t_{s,2}}\right). \tag{3}$$

Variations in the apparent activation energy have an exponential impact on the extrapolated end-of-life of a MOSFET device. The extracted apparent activation energies differ widely and are typically on the order of $E_{a,V}^{app} \approx 0.1$ eV [1], [9] and $E_{a,H}^{app} \approx 1$ eV. In addition, these activation energies strongly depend on bias, stress, and recovery time. The differences are quite dramatic and one might rightfully question the physical significance of these values. This is insofar of fundamental importance as these activation energies have often been used to claim certain physical processes to be responsible for the degradation, e.g., the diffusion of hydrogen [10]–[12].

In the following, we will model BTI using an ensemble of defects following first-order kinetics with distributed capture and emission activation energies E_c and E_e [13]–[18]. For a certain gate voltage, the activation energies of each defect are determined by defect type and position. While both charge trapping and simple bond-breakage reactions have been described using first-order reactions, such distinctions are not necessary once the distribution of activation energies is known. Note that these activation energies can be significantly higher than 1 eV [see Fig. 2(a)]. The resulting time constants are referred to as capture and emission times τ_c and τ_e.

This theoretical framework allows us to discuss the dependence of apparent activation energies on the measurement conditions and describe it mathematically. We show under which conditions these apparent activation energies give reasonable results.

For this purpose, we use previously published model parameters for a 130 nm silicon technology with a 2 nm nitrided gate oxide. The underlying mathematical formulas and the dependence of the apparent activation energies on the point of extraction are presented. We further clarify the role of stress voltage level and recovery time, whereby the latter enters most measurements as the measurement delay time. Finally, we repeat the procedure for a silicon carbide technology and determine the differences and challenges in comparison to silicon. This comparison is insofar revealing as in SiC technologies negative apparent activation energies can be easily observed.

II. Activation Energy Map

An activation energy map (AE map) is a 2-D distribution representing the contribution from different capture and emission activation energies to the overall threshold voltage shift. It was demonstrated that the defect kinetics of each individual defect can be well described by an Arrhenius law [8], [13], [19]

$$\tau = \tau_0 \exp\left(\frac{E_a}{k_B T}\right). \tag{4}$$

Extended MSM (eMSM) schemes with long recovery traces enable the determination of the distribution of capture and emission time constants (CET maps) by numerically calculating the second mixed partial derivative of the threshold voltage shift as a function of stress and recovery time. For further details, please refer to the respective literature [17], [20]. In fact, the resulting distribution extends over several orders of magnitude in time [see Fig. 2(b)]. The capture and emission time constants of each defect are reciprocally linked to the reaction rate of their respective process [13]. Consequently, full recovery is achievable, particularly at higher temperature [9], [21]. Using (4), CET maps at different temperatures allow the extraction of an analytic AE map that is valid for a certain pair of stress and recovery voltages [see Fig. 2(a)]. Voltage-level-dependent models with AE maps have already been proposed [22]. The occurring distribution of activation energies can be described by the superposition of two separate distributions where each of them follows (5) [20], [22]–[24]:

$$g(E_c, E_e) = \frac{A}{2\pi\sigma_c\sigma_{\Delta_e}} \cdot \exp\left(-\frac{(E_c - \mu_c)^2}{2\sigma_c^2} - \frac{(E_e - (rE_c + \mu_{\Delta_e}))^2}{2\sigma_{\Delta e}^2}\right). \tag{5}$$

The model parameter r introduces a correlation between E_c and E_e and can be varied from zero to one [25]. This distribution is a bivariate Gaussian distribution in E_e and E_c, scaled by the factor A, and can be transformed in its standard form by employing the following relations:

$$\mu_e := r\mu_c + \mu_{\Delta e} \tag{6}$$
$$\sigma_e^2 := \sigma_{\Delta e}^2 + r^2\sigma_c^2 \tag{7}$$
$$\rho := r\frac{\sigma_c}{\sigma_e}. \tag{8}$$

The parameters μ_e and σ_e are the mean and the standard deviation of E_e, and ρ is the correlation coefficient. The two distributions constituting the AE map are the recoverable component (R) and the quasi-permanent component (P), based on the time scales related to them. The description of the activation energy distribution with two superimposing bivariate Gaussian distributions allows an analytic approach for the

Authorized licensed use limited to: TU Wien Bibliothek. Downloaded on January 05,2021 at 07:18:06 UTC from IEEE Xplore. Restrictions apply.

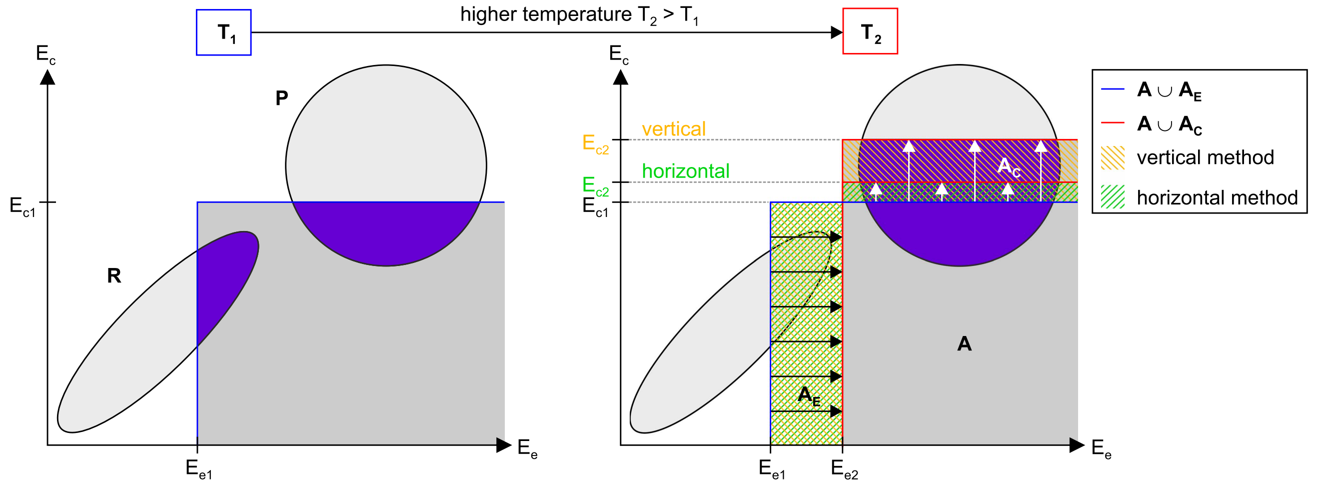

Fig. 3. Schematic of apparent activation energy extraction with the vertical and horizontal method. The stress times at temperature T_1 are chosen to be equal for the two methods. The recovery time is assumed to be the same at both temperatures. Therefore, the measurement at temperature T_1, depicted on the left-hand side, is identical for both methods. At T_1, the threshold voltage shift is obtained by integration of the AE map over the blue framed area. The overlap of the distributions R and P with the integration area is marked in dark gray. The threshold voltage shift at the higher temperature T_2 is obtained by integration over the red framed area on the right-hand side. For the vertical extraction, the freely chosen measurement conditions T_1, T_2, t_s, and t_r determine the quantities E_{c1}, E_{e1}, E_{c2}, and E_{e2} that define the areas A_E, A, and A_c, respectively. The vertical activation energy is determined by integration of the AE map over these areas following (10). Though starting with the identical measurement at T_1, the horizontal extraction is different. While the measurement conditions T_1, T_2, t_{s1}, and t_r are the same as for the vertical method, hence, the respective energies E_{c1}, E_{e1}, and E_{e2} are the same, t_{s2} is determined by the condition $\Delta V_{th}(T_1) = \Delta V_{th}(T_2)$. Consequently, the contribution in area A_E that is lost by increasing the temperature from T_1 to T_2 has to be equal to the contribution from area A_C that is gained by increasing the temperature. As a result, under the condition of a comparably small contribution from A_E and a high amplitude of the distribution around E_{c1}, the area A_C will be small and E_{c2} will be close to E_{c1}. According to (11), the horizontal activation energy will under these circumstances be close to E_{c1}.

calculation of the threshold voltage shift

$$\begin{aligned}\Delta V_{\text{th}}(t_s, t_r) &= \int_0^\infty \int_0^\infty P(\tau_c, \tau_e, t_s, t_r) g(\tau_c, \tau_e)\, d\tau_e\, d\tau_c \\ &= \int_0^\infty \int_0^\infty P(E_c, E_e, t_s, t_r) g(E_c, E_e)\, dE_e\, dE_c \\ &\approx \int_0^{E_{cs}} \int_{E_{er}}^\infty g(E_c, E_e)\, dE_e\, dE_c. \end{aligned} \quad (9)$$

Integration of the product of the AE map with a stress and recovery time-dependent occupation map yields the total threshold voltage shift after specific stress and recovery times. A convenient simplification was performed by approximating $P(E_c, E_e, t_s, t_r) \approx \Theta(E_{cs} - E_c)\Theta(E_e - E_{er})$ in (9), where Θ is the Heaviside step function and E_{er} and E_{cs} are the energies corresponding to the recovery and stress times calculated with (4), respectively. This approximation corresponds to the assumption that all defects with capture times smaller than the stress times are occupied and all defects with emission times smaller than the recovery time are unoccupied.

III. Basic Principles of Apparent Activation Energy Extraction

In general, the threshold voltage shift has to be calculated separately for the recoverable and the quasi-permanent component because the distributions have a different τ_0 relating capture and emission times with the respective energies (see Table I). Since we focus here on the qualitative interpretation of these two extraction schemes, in Section III, τ_0 is assumed to be equal for both components for simplicity.

TABLE I
AE Map Parameters of Fig. 2

	$\tau_0[ns]$	μ_c[eV]	σ_c[eV]	$\mu_{\Delta e}$[eV]	$\sigma_{\Delta e}$[eV]	V_0[V]	m	r
R	$5.55 \cdot 10^{-5}$	0.99	0.314	-0.11	0.216	-0.669	3.05	1
P	0.573	1.27	0.171	1.57	0.211	-0.407	2.77	0

A. Vertical Extraction

Vertical extraction of an apparent activation energy uses the ratio of the threshold voltage shifts at two different temperatures T_1 and T_2 [see (2)]. The stress time (extraction point) and the recovery time, after which the threshold voltage shift is measured, are kept constant. All stress and recovery times correspond to energies in the AE map and are named E_{c1}, E_{e1}, E_{c2} and E_{e2} for the temperatures T_1 and T_2.

In Fig. 3, the principle of the vertical activation energy is illustrated. The energies E_{c1}, E_{e1}, E_{c2}, and E_{e2} are determined by the measurement conditions, such as the stress time, recovery time, and chosen temperatures. These energies span three areas A, A_E, and A_C in the AE map contributing to the threshold voltage shift and determine the vertical activation energy. The threshold voltage shift at T_1 is obtained by integrating the two distributions R and P over the area $A \cup A_E$. For the higher temperature T_2, the integration is performed over the area $A \cup A_C$. If $I(S)$ is the integral of the AE map over the area S, then the vertical activation energy can be written in the following form:

$$E_{a,V}^{app} = k_B \frac{T_1 T_2}{T_2 - T_1} \ln\left(\frac{1 + \frac{I(A_C)}{I(A)}}{1 + \frac{I(A_E)}{I(A)}}\right). \quad (10)$$

Authorized licensed use limited to: TU Wien Bibliothek. Downloaded on January 05,2021 at 07:18:06 UTC from IEEE Xplore. Restrictions apply.

As can be seen above, the vertical activation energy is controlled by the ratios of integrals. As the set of energies $\{E_{c1}, E_{e1}, E_{c2}, \text{and } E_{e2}\}$ is determined by temperature, stress time, and recovery time, the defined integration areas depend on the same parameters. As a result, these parameters determine the apparent vertical activation energy, as discussed later.

B. Horizontal Extraction

For the horizontal activation energy, the same set of energies $\{E_{c1}, E_{e1}, E_{c2}, \text{and } E_{e2}\}$ is used. Given the same recovery times at both temperatures and the same stress time at temperature T_1, only the energy E_{c2} differs from the parameters in the vertical method. E_{c2} is determined by the condition that the threshold voltage shift is equal at both temperatures. This corresponds to varying the integration area A_C in such a way that $I(A_C) = I(A_E)$ is achieved. Straightforward calculations reveal the dependence of the horizontal activation energy on the difference between the parameters E_{c2} and E_{c1}

$$E_{a,H}^{app} = E_{c1} - \underbrace{\frac{T_1}{T_2 - T_1}(E_{c2} - E_{c1})}_{:=\Delta E}. \quad (11)$$

Note that for our particular example, the amplitude A [see (5)] of the quasi-permanent component is more than twice the amplitude of the recoverable component. Regions where the value of the two superimposed distributions is high contribute more to $I(A_C)$. Hence, a small contribution from $I(A_E)$ frequently leads to a small ΔE, and thus, the horizontal activation energy $E_{a,H}^{app}$ approaches E_{c1}. This is the reason why the horizontal activation energy under reasonably long stress times is on the order of the activation energies of the quasi-permanent component.

Due to its dependence on the set of energy parameters and the condition of equal threshold voltage shift, the horizontal activation energy also depends on temperature, stress time, and recovery time.

IV. Analytic Formulation of Apparent Activation Energy Extraction

It is possible to describe the dependence of the apparent activation energies on the measurement parameters mathematically using analytic approximative formulas.

A. Vertical Extraction

Unfortunately, the bivariate Gaussian distribution can, in general, not be integrated in closed form. A very precise approximation for the vertically extracted activation energy in analytical form can be derived by using a formula for the threshold voltage shift suggested previously [23]. A rougher and simpler but more explicit approximation can be obtained by neglecting recovery and approximating the Gaussian profiles with logistic distributions of the same standard

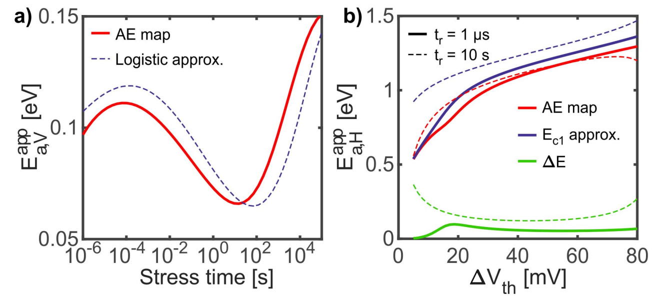

Fig. 4. Analytic approximations for the set of parameters presented in Table I at $V_{GS} = -2$ V: (a) stress time dependence of the vertical activation energy based on an AE map simulation at a recovery time of 1 µs and the logistic approximation from (12). The temperatures are set to be $T_1 = 120$ °C and $T_2 = 150$ °C. (b) Threshold voltage shift dependence of the horizontal activation energy based on AE maps, the horizontal activation energy based on the E_{c1} approximation from (13), and their difference ΔE (see definition in (11)). The recovery times are set to be 1 µs (solid lines) and 10 s (dashed lines) and temperatures are chosen as $T_1 = 120$ °C and $T_2 = 150$ °C. Note that ΔE is small and almost constant over a wide range, particularly at $t_r = 1$ µs.

deviation [20] [see Fig. 4(a)], which gives

$$E_{a,V}^{app} = k_B \frac{T_1\ T_2}{T_2 - T_1} \cdot \ln\left(\frac{\left(1+C_R(T_2)t_s^{-\gamma_R T_2}\right)^{-1} + A\left(1+C_P(T_2)t_s^{-\gamma_P T_2}\right)^{-1}}{\left(1+C_R(T_1)t_s^{-\gamma_R T_1}\right)^{-1} + A\left(1+C_P(T_1)t_s^{-\gamma_P T_1}\right)^{-1}}\right)$$

$$\gamma_i := \frac{\pi k_B}{\sigma_{c,i}\sqrt{3}}, \quad C_i(T) := \exp\left(\frac{\pi \mu_{c,i}}{\sigma_{c,i}\sqrt{3}}\right)\tau_{0,i}^{\gamma_i T}, \ \ i \in \{R, P\}$$

$$A := A_P/A_R. \quad (12)$$

B. Horizontal Extraction

The mathematical treatment of the horizontal method is much more complicated than that of the vertical method. Nevertheless, under the already discussed conditions of a long stress time and a suitably chosen recovery time (see Section III-B), the horizontal activation energy can be approximated by the energy E_{c1} as

$$E_{a,H}^{app} = k_B T_1 \ln\left(\frac{t_{s,1}}{\tau_{0,P}}\right). \quad (13)$$

Equation (13) predicts a logarithmic dependence of the horizontally extracted apparent activation energy on the stress time corresponding to the extraction point at temperature T_1. Consequently, the dependence on the threshold voltage shift is similar. This behavior is very well reproduced in Fig. 4(b). Though ΔE is slightly higher and less constant at longer recovery times, the extraction point E_{c1} dominates the dependence of the horizontal activation energy on the threshold voltage shift.

V. Example I: 130-nm Si-MOSFET

In this section, the dependence of apparent activation energies on different measurement parameters is discussed for a silicon device. As it is common practice, the activation energy extraction is from now on performed by fitting a full Arrhenius

Authorized licensed use limited to: TU Wien Bibliothek. Downloaded on January 05,2021 at 07:18:06 UTC from IEEE Xplore. Restrictions apply.

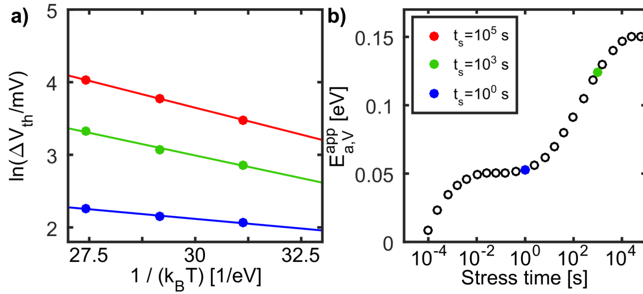

Fig. 5. Vertical extraction method based on experimental data from a silicon technology at a stress voltage of $V_{GS} = -2$ V: (a) Arrhenius plot for the extraction of the activation energy at different stress times with three different temperatures of 100 °C, 150 °C, and 200 °C. (b) Dependence of the apparent activation energy on the stress time for a fixed recovery time of $t_r = 1$ µs. The stress time has a strong influence on the obtained apparent activation energy.

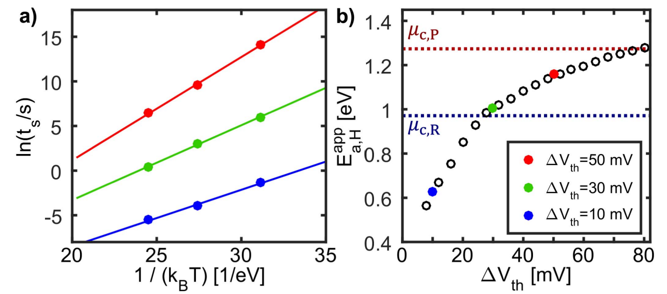

Fig. 6. Horizontal extraction method based on experimental data from a silicon technology at a stress voltage of $V_{GS} = -2$ V. (a) Arrhenius plot for the extraction of the activation energy at different ΔV_{th} with three different temperatures of 100 °C, 150°C, and 200 °C. (b) Dependence of the apparent activation energy on ΔV_{th} for a fixed recovery time of $t_r = 1$ µs. The threshold voltage shift chosen for extraction heavily determines the apparent activation energy.

plot rather than just taking the values of two temperatures, as done for the analytical expressions.

A. Vertical Extraction

The dependence of the vertical activation energy on the stress time at a recovery time $t_r = 1\,\mu$s is shown in Fig. 5. Fig. 5(a) shows the corresponding Arrhenius plot, in which the threshold voltage shift was extracted at three different stress times. Obviously, the apparent activation energy is not the same for the three different stress times, and hence, the respective activation energies are different. The vertical activation energy is plotted versus the stress time in Fig. 5(b). It covers a range from below 0.01 eV up to 0.15 eV for stress times between 10^{-4} s and 10^5 s. A reason for the shape of the curve of the vertical activation energy becomes evident by looking at the AE map in Fig. 2(a); for short stress times, only the defects associated with the recoverable component can be charged and contribute to the threshold voltage shift. In consequence, the activation energy increases until the first plateau in Fig. 5(b) between 10^{-2} s and 1 s. With increasing stress time, the contribution of the quasi-permanent component to the overall threshold voltage shift increases. This explains the increase of the vertically extracted apparent activation energy between 1 s and 10^4 s. Finally, the flattening of the quasi-permanent distribution toward longer stress times leads to a plateau in the extracted activation energy above 10^4 s.

B. Horizontal Extraction

Apparent activation energies obtained by horizontal extraction strongly depend on the measurement parameters. Fig. 6(a) shows the corresponding Arrhenius plot for different threshold voltage shifts where the extraction is performed. Undoubtedly, the activation energy depends on the extraction point, as shown in Fig. 6(b) covering a range from 0.6 up to 1.3 eV. The horizontal method corresponds to measuring the stress time acceleration of the threshold voltage shift contribution of defects around the extraction point. Choosing a higher threshold voltage shift results in higher stress times. Thus, the activation energies are comparable at high threshold voltage shift (around 80 mV) to the mean activation energy μ_c of the quasi-permanent component. A logarithmic dependence on stress time of the apparent activation energy at high threshold voltage shifts helps to reduce the deviation from the mean μ_c of the quasi-permanent component. Nonetheless, the already presented calculations make clear that this only provides a rough estimate and does not replace the use of a whole AE map.

C. Comparison Vertical/Horizontal Extraction

As the vertical activation energy is not a physically justified quantity, it is not surprising that their values differ considerably from the energies shown in the AE map (see Fig. 2). Under the assumption that the power law of (1) fits the measurement data with a temperature dependence

$$\Delta V_{\mathrm{th}} \propto \exp\left(-\frac{E_{\mathrm{a,V}}^{\mathrm{app}}}{k_{\mathrm{B}}T}\right) \tag{14}$$

the horizontal activation energy can be calculated by dividing the vertical activation energy by the time exponent n

$$E_{\mathrm{a,H}}^{\mathrm{app}} = \frac{E_{\mathrm{a,V}}^{\mathrm{app}}}{n}. \tag{15}$$

Under the above assumptions, modeling the temperature dependence based on horizontal or vertical activation energies is completely equivalent to a correct description. However, the energy values differ strongly. For typical values of n, the horizontal activation energy is roughly three-to-ten times the vertical activation energy. As the horizontal activation energy is more likely in the range of the quasi-permanent component, the physical meaning of the vertical activation energy can partly be restored by using (15). Note that n is no physical parameter either and just based on a power-law fit.

Typical stress times in industrial device qualification are in the range of 2000 h $= 7.2 \times 10^6$ s. Considering the present exemplary technology, temperatures $T_1 = 120\,°$C and $T_2 = 150\,°$C will yield a threshold voltage shift of around 62 mV with an activation energy of 1.20 eV at a recovery time of 10 s. Although the stress time corresponds to an energy $E_{c2} = 1.35$ eV, which is above the center $\mu_c = 1.27$ eV of the quasi-permanent component, this result is very close to

Authorized licensed use limited to: TU Wien Bibliothek. Downloaded on January 05,2021 at 07:18:06 UTC from IEEE Xplore. Restrictions apply.

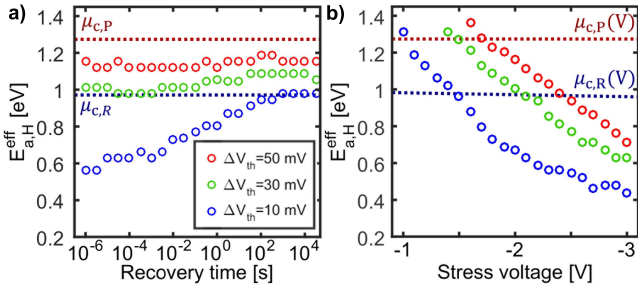

Fig. 7. Horizontal extraction method with a silicon technology. (a) Dependence of the apparent activation energy on the recovery time at a stress voltage of $V_{GS} = -2$ V at different values of ΔV_{th}. Choosing higher threshold voltage shifts reduces the recovery dependence. (b) Dependence of the apparent activation energy on the stress voltage at different values of ΔV_{th} based on experimental data and AE map simulations. Due to the increasing contribution of *R*, the higher the absolute value of the stress voltage, the lower the extracted apparent activation energy.

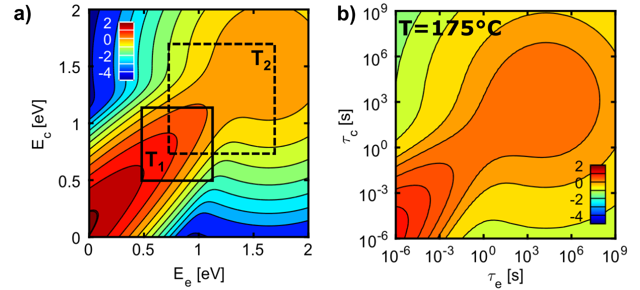

Fig. 8. AE and CET maps extracted for a silicon carbide trench MOSFET test device (data and further details presented in [29]) for $V_{GS} = 25$ V. Both maps are shown on a logarithmic color scale. A density value of *x* corresponds to ΔV_{th} of 10^{x} Vev and 7×10^{x} mV. (a) AE map for the recoverable and quasi-permanent component. The squares indicate the measurement windows of the two temperatures T_1 and T_2 used to create the AE map. Analogously to the silicon technology, the distribution is described by a superposition of two Gaussian distributions (see (5)) and the same set of parameters (see Table I). (b) Capture and emission time map at $T = 175$ °C calculated from (a). Note that the shown density values are per squared decade in time.

$\mu_c = 1.27$ eV. In contrast to that, the vertical activation energy at the same stress time would yield a value of 0.15 eV.

D. Influence of Recovery

Recovery is a known parameter influencing the measured threshold voltage shift and, thus, the extracted activation energy [9]. This dependence is illustrated for the horizontal extraction of an apparent activation energy. Fig. 7(a) shows the activation energy versus the recovery time for three different extraction points. The lowest extraction point of 10 mV exhibits the strongest dependence on the recovery time. This dependence is minimized for the highest extraction point of 50 mV. Certainly, the reason for this behavior is the reduction of the relative contribution of the recoverable component to the total threshold voltage shift. By increasing the extraction point and, thus, the stress time, the quasi-permanent component with its high amplitude increasingly dominates the total threshold voltage shift. Thereby, recovery at time scales of the recoverable component loses its influence. The extraction of the activation energy is increasingly dominated by the temperature dependence of the quasi-permanent component, where recovery on time scales of the recoverable component is negligible.

E. Influence of Stress Voltage

The stress voltage dependence of AE maps was already successfully described and modeled previously [22], [23] by making the amplitudes of the recoverable and the quasi-permanent distributions bias-dependent as $A = (V_{GS}/V_0)^m$ mV eV^{-2}. It was also observed that the mean values μ_c of the capture activation energy become linearly smaller with increasing absolute value of the stress voltage. However, this effect was found to be negligible as the mean energy changes only by 0.01 eV V^{-1} for the recoverable component and is virtually constant for the quasi-permanent component. Note that a small stress voltage dependence of the mean values μ_c of the distributions in the AE map does not allow to conclude a small voltage dependence of single defects [23], [26], because a change in stress voltage changes also the defects contributing to BTI.

Fig. 7(b) shows the dependence of the horizontal activation energy on the stress voltage for three different extraction points. For all three cases, the extracted activation energy decreases almost linearly with increasing absolute value of the stress voltage. An increased stress voltage leads to a decreased stress time for the same threshold voltage shift. As already shown even under ideal conditions at long stress times, the horizontal activation energy depends on the stress time itself [see (13)]. The impact of a reduced stress time is a reduced apparent activation energy. Therefore, increasing the stress voltage is not a good means for the acceleration of measurements.

VI. Example II: SiC Trench-MOSFET Test Device

It has been shown previously that AE maps can also be applied to SiC Trench MOSFETs to capture both NBTI and PBTI in a unified manner [27], [28].

The AE map and a CET map at 175 °C of a SiC Trench MOSFET test device are shown in Fig. 8. A major difference to Si devices is the dominating contribution from defects with short capture and emission time constants. To clarify, the observation that the mean μ_e of the recoverable component seems to be negative is explained by the fact that these defects are difficult to detect in threshold voltage measurements. A shortest measurable recovery time of 1 µs is not sufficient to fully capture the distribution of the recoverable component toward the coordinate origin. Consequently, the extrapolation toward short time constants of fitted data in the measurement window with a Gaussian distribution is spurious; nevertheless, the results are completely in accordance with measurement data above the shortest measurable recovery time. Due to the comparably high concentration of active defects with short time constants, the contribution of the recoverable component to the overall threshold voltage shift can mostly not be neglected. Therefore, just like in Si devices, the recovery time is of major importance for the interpretation of measurements on SiC devices. For short recovery times, an increase in temperature can lead to a faster increase in recovery than

Authorized licensed use limited to: TU Wien Bibliothek. Downloaded on January 05,2021 at 07:18:06 UTC from IEEE Xplore. Restrictions apply.

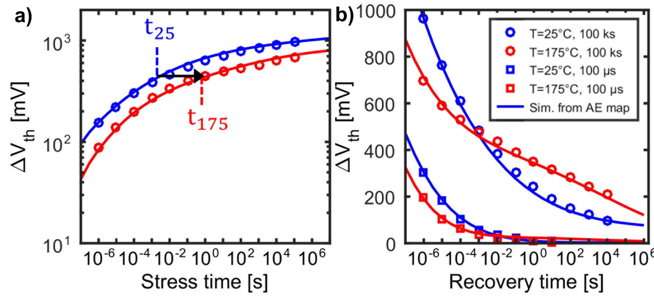

Fig. 9. Measured threshold voltage shift ΔV_{th} from a silicon carbide technology with a stress voltage of $V_{GS} = 25$ V at two different temperatures. Solid lines indicate the drift values resulting from a simulation based on the AE map in Fig. 8. (a) Measured threshold voltage shift and the corresponding simulation at two different temperatures versus the stress time. The recovery time is 1 µs. Interestingly, at a higher temperature, a reduced threshold voltage shift is obtained. (b) Measured and simulated threshold voltage shift at different temperatures with different stress times versus the recovery time. The recovery traces have an intersection point at which the polarity of the apparent activation energy changes.

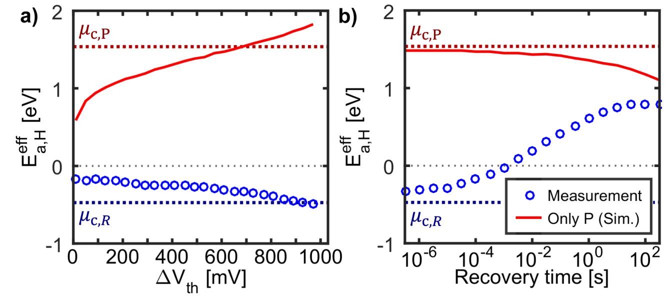

Fig. 10. Horizontal extraction of the apparent activation energy based on experimental data from a silicon carbide test device at a stress voltage of $V_{GS} = 25$ V: (a) extracted apparent activation energy and the simulated activation energy in the absence of R versus ΔV_{th}. The dependence is similar to silicon technologies if only P is considered. (b) Extracted apparent activation energy and the simulated activation energy in the absence of R versus the recovery time at a ΔV_{th} of 700 mV. The intersection point of the recovery traces in Fig. 9(b) determines the point of change in sign of the extracted apparent activation energy.

during stress, resulting in an apparently smaller threshold voltage shift and, therefore, a negative apparent activation energy. Such an activation energy is of course nonphysical and underlines the necessity of using complete AE maps to understand the relevant defect distributions. As the vertical method has already shown to be extremely nonphysical, we restrict the discussion in the following to the horizontal method.

A. Horizontal Extraction

Due to the large concentration of fast recoverable defects, SiC devices can exhibit negative apparent activation energies. Fig. 9(a) shows the threshold voltage shift after positive gate stress for temperatures of 25 °C and 175 °C. These measurements were performed with a recovery time of 1 µs. A higher temperature leads to a smaller threshold voltage shift. Such a decreasing voltage shift with increasing temperature implies a negative apparent activation energy. Fig. 9(b) shows the recovery traces for these two temperatures for the stress times 100 µs and 100 ks. Apparently, this effect of negative apparent activation energy emerges at short recovery times. The polarity of the apparent activation energy depends on whether the measurement delay is below or above the intersection of the recovery traces of different temperatures. For a stress time of 100 µs, this is above 1 s. For 100 ks, the intersection is at around 1 ms. Consequently, even the polarity of both the vertical and the horizontal apparent activation energy depends on recovery and stress time.

Fig. 10 shows the horizontal activation energy in dependence on either the extraction point or the recovery time. The measurement data at a recovery time of 1 µs show negative activation energies for the whole range of extraction points. A comparison of the AE map of the presented Si device in Fig. 2 and the one of the SiC trench test device in Fig. 8 provides an explanation. According to (4), some defects will move out of the measurement window as their emission time constant becomes lower than the recovery time, so that they do not contribute to the threshold voltage shift anymore. For SiC, it is possible that the contribution of additionally charged defects at higher temperature is lower than the lost contribution from defects that moved out of the measurement window. This leads to a lower threshold voltage shift at higher temperature for a fixed recovery time and, thus, to a negative apparent activation energy. With increasing recovery time, the initially dominant recoverable component recovers and the apparent activation energy changes its sign.

Aichinger *et al.* [30] and Rescher *et al.* [31] provided a solution using device preconditioning. This method essentially leads to the removal of the contribution of the recoverable component to the threshold voltage shift by applying discharging pulses toward accumulation prior to measurements to reveal the quasi-permanent component. As a result, reproducible measurements and extrapolation to end-of-life, using only the quasi-permanent component, are possible.

VII. Discussion and Conclusion

The findings of this study demonstrate that in the context of BTI, regardless of which extraction method is employed, apparent activation energies are not able to describe the temperature dependence of BTI which is actually determined by a wide distribution of activation energies. Apparent activation energies are especially vulnerable to their point of extraction. Depending on the extraction method, this is either the threshold voltage shift (horizontal method) or the stress time (vertical method). As the deviation of the apparent activation energy from the mean μ_c of the quasi-permanent component can exceed 50% for the horizontal and even 99% for the vertical extraction method, the dependence on the extraction point cannot be neglected.

Vertical extraction results in small activation energies that are completely uncorrelated to physically meaningful values. The dependence of the activation energy on the stress time reflects the two bivariate Gaussian distributions, while the observed plateaus do not provide sensible values.

Horizontal extraction, on the other hand, leads to values that are closer to the mean activation energy μ_c of the quasi-permanent component. While this can only be achieved at long stress times, the horizontal method should be clearly preferred to the vertical method. Results should be considered carefully as they are not related to the mean activation energy μ_c of the quasi-permanent component but rather directly to the extraction point.

Authorized licensed use limited to: TU Wien Bibliothek. Downloaded on January 05,2021 at 07:18:06 UTC from IEEE Xplore. Restrictions apply.

Recovery is a further factor influencing the outcome of apparent activation energy extraction. Its impact on the activation energy can again be minimized by employing a high extraction threshold voltage shift.

Strikingly, silicon carbide MOSFET devices show an even stronger influence of extraction point and recovery time. In this case, the activation energy can even change its sign depending on the recovery time. Therefore, it is essential to either extract the full AE map or to at least work with device preconditioning, leading to discharging of defects with short time constants.

The results of this study are highly relevant for the discussion on the physical origin of BTI. Previous reports on the temperature dependence of BTI have to be considered with caution because commonly used different extraction methods lead to unphysical apparent activation energies. Our analysis clearly shows that studies trying to identify the physical origin of BTI have to be aware of the dependencies of single-value activation energies on their underlying distributions and consequently of the physical insignificance of these values. Industrial device qualification using apparent activation energies is insofar concerned as adequate end-of-life modeling requires a correct description of the temperature dependence of BTI.

References

[1] M. Denais *et al.*, "Interface traps and oxide traps under NBTI and PBTI in advanced CMOS technology with a 2 nm gate-oxide," in *Proc. IEEE Int. Integr. Rel. Workshop Final Rep.*, Oct. 2003, pp. 1–6, doi: 10.1109/IRWS.2003.1283289.

[2] S. Chakravarthi, A. Krishnan, V. Reddy, C. F. Machala, and S. Krishnan, "A comprehensive framework for predictive modeling of negative bias temperature instability," in *Proc. IEEE Int. Rel. Phys. Symp.*, Apr. 2004, pp. 273–282, doi: 10.1109/RELPHY.2004.1315337.

[3] D. Varghese, D. Saha, S. Mahapatra, K. Ahmed, F. Nouri, and M. Alam, "On the dispersive versus arrhenius temperature activation of nbti time evolution in plasma nitrided gate oxides: Measurements, theory, and implications," in *IEDM Tech. Dig.*, Dec. 2005, pp. 684–687, doi: 10.1109/IEDM.2005.1609444.

[4] G. Rzepa *et al.*, "Comphy—A compact-physics framework for unified modeling of BTI," *Microelectron. Rel.*, vol. 85, pp. 49–65, Jun. 2018, doi: 10.1016/j.microrel.2018.04.002.

[5] S. Zafar, B. H. Lee, and J. Stathis, "Evaluation of NBTI in HfO_2 gate-dielectric stacks with tungsten gates," *IEEE Electron Device Lett.*, vol. 25, no. 3, pp. 153–155, Mar. 2004, doi: 10.1109/LED.2004.824244.

[6] B. Kaczer *et al.*, "Ubiquitous relaxation in BTI stressing—New evaluation and insights," in *Proc. IEEE Int. Rel. Phys. Symp.*, Apr. 2008, pp. 20–27, doi: 10.1109/RELPHY.2008.4558858.

[7] K. Puschkarsky, T. Grasser, T. Aichinger, W. Gustin, and H. Reisinger, "Review on SiC MOSFETs high-voltage device reliability focusing on threshold voltage instability," *IEEE Trans. Electron Devices*, vol. 66, no. 11, pp. 4604–4616, Nov. 2019, doi: 10.1109/TED.2019.2938262.

[8] K. Puschkarsky, H. Reisinger, C. Schlunder, W. Gustin, and T. Grasser, "Fast acquisition of activation energy maps using temperature ramps for lifetime modeling of BTI," in *Proc. 48th Eur. Solid-State Device Res. Conf. (ESSDERC)*, Sep. 2018, pp. 218–221, doi: 10.1109/ESSDERC.2018.8486855.

[9] S. Rangan, N. Mielke, and E. C. C. Yeh, "Universal recovery behavior of negative bias temperature instability [PMOSFETs]," in *IEDM Tech. Dig.*, Dec. 2003, pp. 14.3.1–14.3.4, doi: 10.1109/IEDM.2003.1269294.

[10] K. O. Jeppson and C. M. Svensson, "Negative bias stress of MOS devices at high electric fields and degradation of MNOS devices," *J. Appl. Phys.*, vol. 48, no. 5, pp. 2004–2014, May 1977, doi: 10.1063/1.323909.

[11] M. A. Alam and S. Mahapatra, "A comprehensive model of PMOS NBTI degradation," *Microelectron. Rel.*, vol. 45, no. 1, pp. 71–81, Jan. 2005, doi: 10.1016/j.microrel.2004.03.019.

[12] M. A. Alam, H. Kufluoglu, D. Varghese, and S. Mahapatra, "A comprehensive model for PMOS NBTI degradation: Recent progress," *Microelectron. Rel.*, vol. 47, no. 6, pp. 853–862, Jun. 2007, doi: 10.1016/j.microrel.2006.10.012.

[13] H. Reisinger, T. Grasser, W. Gustin, and C. Schlunder, "The statistical analysis of individual defects constituting NBTI and its implications for modeling DC- and AC-stress," in *Proc. IEEE Int. Rel. Phys. Symp.*, May 2010, pp. 7–15, doi: 10.1109/IRPS.2010.5488858.

[14] T. Grasser, K. Rott, H. Reisinger, M. Waltl, F. Schanovsky, and B. Kaczer, "NBTI in nanoscale MOSFETs—The ultimate modeling benchmark," *IEEE Trans. Electron Devices*, vol. 61, no. 11, pp. 3586–3593, Nov. 2014, doi: 10.1109/TED.2014.2353578.

[15] G. Rzepa *et al.*, "Physical modeling of NBTI: From individual defects to devices," in *Proc. Int. Conf. Simulation Semiconductor Processes Devices (SISPAD)*, Sep. 2014, pp. 81–84, doi: 10.1109/SISPAD.2014.6931568.

[16] B. Kaczer *et al.*, "NBTI from the perspective of defect states with widely distributed time scales," in *Proc. IEEE Int. Rel. Phys. Symp.*, Apr. 2009, pp. 55–60, doi: 10.1109/IRPS.2009.5173224.

[17] T. Grasser, "Stochastic charge trapping in oxides: From random telegraph noise to bias temperature instabilities," *Microelectron. Rel.*, vol. 52, no. 1, pp. 39–70, Jan. 2012, doi: 10.1016/j.microrel.2011.09.002.

[18] G. Pobegen and T. Grasser, "On the distribution of NBTI time constants on a long, temperature-accelerated time scale," *IEEE Trans. Electron Devices*, vol. 60, no. 7, pp. 2148–2155, Jul. 2013, doi: 10.1109/TED.2013.2264816.

[19] G. Pobegen, T. Aichinger, M. Nelhiebel, and T. Grasser, "Understanding temperature acceleration for NBTI," in *IEDM Tech. Dig.*, Dec. 2011, pp. 614–617, doi: 10.1109/IEDM.2011.6131623.

[20] T. Grasser, "The capture/emission time approach to the bias temperature instability," in *Bias Temperature Instability for Devices and Circuits*, T. Grasser, Ed. New York, NY, USA: Springer, 2014, pp. 447–481.

[21] A. A. Katsetos, "Negative bias temperature instability (NBTI) recovery with bake," *Microelectron. Rel.*, vol. 48, no. 10, pp. 1655–1659, Oct. 2008, doi: 10.1016/j.microrel.2008.04.012.

[22] K. Puschkarsky, H. Reisinger, C. Schlunder, W. Gustin, and T. Grasser, "Voltage-dependent activation energy maps for analytic lifetime modeling of NBTI without time extrapolation," *IEEE Trans. Electron Devices*, vol. 65, no. 11, pp. 4764–4771, Nov. 2018, doi: 10.1109/TED.2018.2870170.

[23] T. Grasser *et al.*, "Analytic modeling of the bias temperature instability using capture/emission time maps," in *IEDM Tech. Dig.*, Dec. 2011, pp. 618–621, doi: 10.1109/IEDM.2011.6131624.

[24] K. Puschkarsky, H. Reisinger, G. A. Rott, C. Schlunder, W. Gustin, and T. Grasser, "An efficient analog compact NBTI model for stress and recovery based on activation energy maps," *IEEE Trans. Electron Devices*, vol. 66, no. 11, pp. 4623–4630, Nov. 2019, doi: 10.1109/TED.2019.2941889.

[25] Y. Illarionov *et al.*, "Hot-carrier degradation and bias-temperature instability in single-layer graphene field-effect transistors: Similarities and differences," *IEEE Trans. Electron Devices*, vol. 62, no. 11, pp. 3876–3881, Nov. 2015, doi: 10.1109/TED.2015.2480704.

[26] T. Grasser, H. Reisinger, P.-J. Wagner, F. Schanovsky, W. Goes, and B. Kaczer, "The time dependent defect spectroscopy (TDDS) for the characterization of the bias temperature instability," in *Proc. IEEE Int. Rel. Phys. Symp.*, May 2010, pp. 16–25, doi: 10.1109/IRPS.2010.5488859.

[27] G. Pobegen and T. Grasser, "Efficient characterization of threshold voltage instabilities in SiC nMOSFETs using the concept of capture-emission-time maps," *Mater. Sci. Forum*, vols. 740–742, pp. 757–760, Jan. 2013, doi: 10.4028/www.scientific.net/MSF.740-742.757.

[28] K. Puschkarsky, H. Reisinger, T. Aichinger, W. Gustin, and T. Grasser, "Understanding BTI in SiC MOSFETs and its impact on circuit operation," *IEEE Trans. Device Mater. Rel.*, vol. 18, no. 2, pp. 144–153, Jun. 2018, doi: 10.1109/TDMR.2018.2813063.

[29] K. Puschkarsky, T. Grasser, T. Aichinger, W. Gustin, and H. Reisinger, "Understanding and modeling transient threshold voltage instabilities in SiC MOSFETs," in *Proc. IEEE Int. Rel. Phys. Symp. (IRPS)*, Mar. 2018, pp. 3B.5-1–3B.5-10, doi: 10.1109/IRPS.2018.8353560.

[30] T. Aichinger, G. Rescher, and G. Pobegen, "Threshold voltage peculiarities and bias temperature instabilities of SiC MOSFETs," *Microelectron. Rel.*, vol. 80, pp. 68–78, Jan. 2018, doi: 10.1016/j.microrel.2017.11.020.

[31] G. Rescher, G. Pobegen, T. Aichinger, and T. Grasser, "Preconditioned BTI on 4H-SiC: Proposal for a nearly delay time-independent measurement technique," *IEEE Trans. Electron Devices*, vol. 65, no. 4, pp. 1419–1426, Apr. 2018, doi: 10.1109/TED.2018.2803283.

Authorized licensed use limited to: TU Wien Bibliothek. Downloaded on January 05,2021 at 07:18:06 UTC from IEEE Xplore. Restrictions apply.